

Crystallinity and perfection in ethylene vitrimers probed by combined calorimetry, scattering, and time-domain NMR

- 1 Kay Saalwächter^{1*}, Bhaskar Soman^{2,3}, Christopher M. Evans^{2,3*}
- ¹Department of Materials Science and Engineering, Urbana, Illinois 61801, USA
- ²Frederick Seitz Materials Research Laboratory, Urbana, Illinois 61801, USA
- 4 ³Institut für Physik NMR, Martin-Luther-Universität Halle-Wittenberg, 06099 Halle (Saale),
- 5 Germany
- 6 * Correspondence:
- 7 Corresponding Authors
- 8 kay.saalwaechter@physik.uni-halle.de
- 9 cme365@illinois.edu
- 10 Keywords: covalent adaptive networks, polymer crystallization, crystallization kinetics,
- polymorphism, memory effect, superheating
- 12 Abstract
- 13 The kinetics of crystallization and crystal-crystal transformations in ethylene vitrimers are studied by
- time-domain NMR. These vitrimers previously exhibited polymorphic transition of crystal structures.
- which are shown here to be distinguishable by NMR via their dipolar line widths based upon
- different proton densities. The conditions under which the polymorphs are formed and interconvert
- are identified via time-resolved NMR experiments, with a focus on recrystallization after full and
- partial melting. The DSC experiments are used to clarify an unexpected superheating effect, which
- challenges the determination of actual melting points. We further identify a strong memory effect in
- 20 isothermal (re)crystallization. Implications of the dynamic nature of the vitrimers in relation to the
- 21 kinetics of crystallization are discussed.

22 1 Introduction

- 23 Covalent adaptable networks (CANs) are polymer networks crosslinked using dynamic covalent
- bonds (Kloxin and Bowman, 2013). Their ability to be reprocessed and recycled have made them
- 25 prime candidates for the next generation of sustainable plastics. Vitrimers are a sub-category of
- 26 CANs where the network strands are crosslinked by associative covalent bonds. (Montarnal et al.,
- 27 2011; Guerre et al., 2020; Van Zee and Nicolay, 2020; Zheng et al., 2021) These bonds undergo
- 28 exchange reactions such that the overall crosslink density of the networks is conserved during the
- 29 exchange. The bond exchange adds a degree of freedom on the molecular scale, that has a strong
- 25 exchange. The bond exchange dads a degree of freedom on the molecular scale, that has a strong
- impact on macroscopic properties. A core question in the study of vitrimers has been to understand
- 31 how parameters like molecular weight, molecular weight dispersity, junction chemistry, backbone
- 32 chemistry, temperature, and crosslink density impact macroscopic properties such as viscosity, stress
- relaxation, creep, reprocessability, and self-healing ability (Denissen et al., 2015; Denissen et al.,
- 34 2017; Röttger et al., 2017; El-Zaatari et al., 2020; Hubbard et al., 2021; Ishibashi et al., 2021; Porath
- and Evans, 2021; Ricarte and Shanbhag, 2021; Hubbard et al., 2022; Krishnan et al., 2022; Luo et al.,

- 36 2022; Porath et al., 2022). In recent years, using the knowledge generated from numerous
- 37 fundamental studies, functional vitrimers have been developed for wide-ranging applications such as
- 38 solid polymer electrolytes, durable coatings, shape-memory materials, and additive manufacturing
- 39 (Jing and Evans, 2019; Yan et al., 2020; Chen et al., 2021; Ma et al., 2021; Niu et al., 2021;
- 40 Rossegger et al., 2021; Gu et al., 2022; Lin et al., 2022; Van Lijsebetten et al., 2022) Despite the
- advances in vitrimers design and processing, a good understanding of how an exchange event that 41
- 42 takes place on an Angstrom scale influences macroscopic events such as crystallization, rheological
- 43 flow and self-assembly is lacking. Little work has focused on how adding dynamic bonds will affect
- 44 the ability of polymer chains to crystallize (Soman et al., 2022a; Kuenstler and Bowman, 2023),
- which is a key attribute of polyolefins and many commercial plastics. 45
- 46 Most work on vitrimers has used rheology or dynamic mechanical analysis to study the moduli and
- flow properties of the networks (Yan et al., 2020; Chen et al., 2021; Ma et al., 2021; Niu et al., 2021; 47
- 48 Gu et al., 2022; Lin et al., 2022; Van Lijsebetten et al., 2022). Some work has also utilized dielectric
- 49 spectroscopy to probe segmental scale dynamics (Soman et al., 2022b; Pascual-Jose et al., 2023).
- While these methods can probe materials which are crystallizing, they are not routinely used to 50
- 51 understand such processes and to infer quantities such as percent crystallinity or the degree of crystal
- 52 perfection (Wurm et al., 2005; Soccio et al., 2007; Ezquerra et al., 1994) Solid-state NMR
- 53 spectroscopy provides a plethora of techniques which can provide a great deal of insight regarding
- 54 crystallization physics in soft materials (Chen and Kurosu, 2007). This holds in particular for proton
- 55 NMR, possibly performed on cost-efficient low-field low-resolution instruments, which allows for a
- 56 quick mobility-based determination of the absolute crystallinity (in terms of proton signal fraction,
- 57 equaling mass fraction), provides access to domain sizes via spin diffusion, and importantly, has
- 58 sufficient sensitivity to allow for time-resolved experiments with a resolution of less than a minute
- 59 (Tanaka and Nishi, 1986; Maus et al., 2006; Schäler et al., 2015). Work along these lines is relevant
- 60 beyond the field of vitrimers, as crystallization in networks, in particular highly crosslinked ones, is
- little researched and understood in general (Golitsyn et al., 2019). The cited paper reports on one of 61
- 62 the few systematic studies of model networks with short but defined network chain length, where the
- normally highly crystallinity of polyethylene oxide (PEO) linear polymers (typically 80% or higher) 63
- 64 is significantly reduced in end-linked networks with chains of less than a few kDa. Tightly
- crosslinked thermosets are mostly amorphous, as are the covalent equivalents of the samples studied 65
- herein (Soman et al., 2022a). A peculiar exception seems to be urea/formaldehyde resins, which can 66
- 67
- reach crystallinities in the 50% range (Wibowo and Park, 2020). This, however, seems to be a special
- 68 case where for the given small-molecule-based resin formulation, crystallization of linear stretches
- 69 and crosslinking compete already during curing.
- 70 To sum up our recent work relevant for the given follow-up study, the role of dynamic bond
- exchange on crystallization in networks has been investigated in ethylene vitrimers (Soman et al., 71
- 72 2022a). They are comprised of monodisperse telechelic alkane diols (CH₂)_n(OH)₂, with n being 10
- 73 and 12 in this work, crosslinked by boric acid, B(OH)₃, samples with exact linker spacing were
- synthesized. The samples are denoted C₁₀ and C₁₂, respectively. In comparison to analogous, 74
- 75 permanently crosslinked networks, which do not show any evidence of crystallization, ethylene
- 76 vitrimers did crystallize with local packing motifs analogous to those of polyethylene (PE). At room
- temperature, crystallization was previously followed over 30 days, and the melting temperature of the 77
- 78 crystals continuously increased by ~25 degrees, while crystallinity as reflected in the DSC-detected
- 79
- melting enthalpy remained nearly constant. While the absolute crystallinity was not yet quantified,
- 80 wide-angle X-ray scattering (WAXS) suggested rather high crystallinity indicated by the virtual
- 81 absence of an amorphous halo and high thermal conductivity. WAXS further revealed an unexpected
- 82 crystal-crystal transition which indicated a second crystal polymorph. It is interesting to note that

- these changes in properties take place in quiescent samples. We attributed the initial crystallization
- and the subsequent evolution in properties to the dynamic bonds. Local rearrangements of the
- 85 network strands facilitated by bond exchange are hypothesized to allow crystal perfection or an
- 86 increase in crystallinity, and to enable a crystal-crystal transformation into a more stable polymorph.
- 87 Even more recent work by Kuenstler and Bowman (2023) have also investigated crystallization in
- 88 dynamic networks, where different catalysts allowed for control of bond exchange kinetics. A similar
- long-time evolution in $T_{\rm m}$ was observed, and the actual $T_{\rm m}$ values were found to be inversely
- 90 correlated with the exchange kinetics.
- Here we investigate in more detail the crystallization of the recently reported high-crosslink-density
- ethylene vitrimer (Soman and Evans, 2021; Soman et al., 2022a; Soman et al., 2022b; Lv et al.,
- 93 2023). We focus on the kinetics of isothermal crystallization as well as the annealing/recrystallization
- 94 kinetics of two different samples with C₁₀ and C₁₂ spacer length. Along the lines of earlier work on
- 95 the confined crystallization of pharmaceuticals (Sonnenberger et al., 2016), we are able to distinguish
- two different crystal polymorphs by simple ¹H NMR via their dipolar line width, allowing us to
- 97 monitor the interconversion in real time. Interestingly, we could identify an unexpected superheating
- 98 effect, which challenges the determination of the melting points reported previously for our samples,
- as well as a prominent memory effect on crystallization.

100 2 Materials

104

- The samples investigated in this work are prepared via the condensation of alkane diols with boric
- acid. The synthetic procedure follows exactly from our prior work (Soman et al., 2022a)

103 3 Results and Discussion

3.1 Samples and rheological characterization

- The previously investigated and carefully dried C_{10} and C_{12} ethylene vitrimers were prepared in
- sealed glass tubes flushed with Argon for NMR measurements. We refer to our previous publication
- for details (Soman and Evans, 2021). The structure of the dynamic networks is shown as in inset in
- Figure 1a, where we have compiled the terminal relaxation times of these samples. The rheological
- measurements were already done in the context of our first publication from which the Arrhenius
- slopes were determined, but the relaxation times of C_{10} and C_{12} were not explicitly published there.
- The data shows that the networks relax on a 0.1 1 s timescale in the temperature range relevant for
- the present study. This will be taken up in the discussion below.

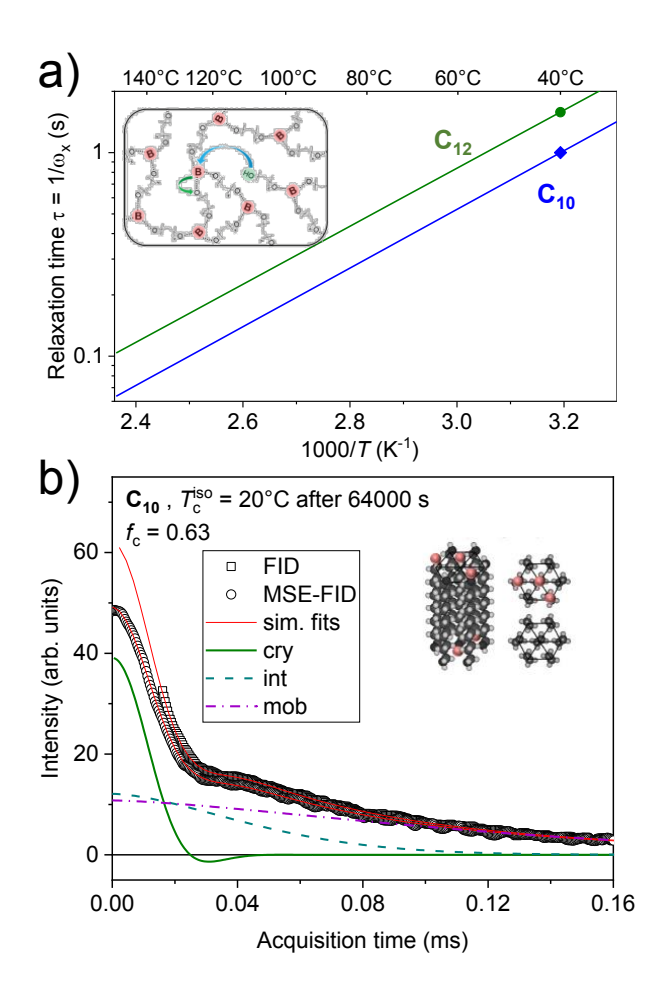


Figure 1. a) Arrhenius plot of vitrimer relaxation times calculated as the inverse of the rheological crossover frequency of samples C_{10} and C_{12} measured at 40°C along with extrapolations based upon shift factors (data taken from Soman et al., 2021). The inset shows the network structure. b) Simultaneous three-component fit of ¹H FIDs, detected during isothermal crystallization at 20°C, both directly after the excitation pulse and after an MSE to avoid the dead time. The fits provide the crystalline fraction (f_c) and second moments of the corresponding crystalline lineshapes (M_2), as well as T_2 relaxation times characterizing the restricted mobility of the intermediate and amorphous fractions. The inset shows the hexagonal crystal structure formed under the given condition (Soman et al., 2022a)

3.2 Differential scanning calorimetry (DSC)

Samples (2-5 mg) were melted into hermetically sealed pans in an Argon glovebox. Crystallization proceeded in the glovebox at ambient temperature. A TA Instruments DSC 25 was used to control the heating and cooling rates as described in the text.

3.3 Combined small- and wide-angle X-ray scattering (SAXS/WAXS)

Samples were prepared for X-ray analysis by sealing between two Kapton sheets using epoxy and a spacer. A Xenocs GeniX3D Cu K α source generated 1.54 Å X-rays and scattering was recorded on a Pilatus 1M detector. Sample-to-detector distance was calibrated using silver behenate, and 2D data was azimuthally averaged using a MATLAB-based GIXSGUI software to determine intensity as a function of wavevector q.

3.4 NMR spectroscopy and data analysis

- 133 NMR experiments were conducted on a Bruker minispec mg20 instrument at a Larmor frequency of
- 134 about 20 MHz. Pulse lengths were in a range of 2.5 and 5 µs for flip angles of 90° and 180°,
- respectively. A recycle delay of 1 s was sufficient for full T_1 relaxation of both semicrystalline and 135
- 136 amorphous/molten samples. The free induction decay (FID) of the proton signal is measured both
- 137 directly and after a magic-sandwich echo (MSE-FID) to address the dead-time problem (Maus et al.,
- 138 2006; Schäler et al., 2015). The latter suffers some intensity loss, which means that we fit the two
- 139 datasets (restricted to an acquisition time interval of 200 ms) simultaneously to a three-component
- 140 model accounting for the crystalline (index c), amorphous (a), and interfacial (i) regions (Schäler et
- 141 al., 2015):

132

161

162

$$I(t) = A_c e^{-(at)^2/2} \sin(bt)/(bt) + A_i e^{-(t/T_{2i})^{\beta_i}} + A_m e^{-(t/T_{2m})^{\beta_m}}$$

- 143 The MSE leads to a small reduction of the amplitude prefactors, which are the only fitting parameters
- 144 that are allowed to vary between FID and MSE-FID signals. Sample fits are shown in Figure 1b.
- Most importantly, these fits provide the crystalline fraction $(f_c = A_c/(A_c + A_i + A_m))$, using the 145
- amplitudes of the undistorted FID. Since NMR intensities are strictly proportional to proton fractions, 146
- 147
- f_c reflects crystallinity by weight. Information on the crystal packing is obtained in terms of the second moment of the crystalline lineshape $(M_2 = a^2 + b^2/3)$, which depends on the overall 148
- 149 strength of multi-proton dipole-dipole interactions as governed by their proximity, i.e. the density. It
- 150 thus reflects the crystalline perfection of the sample.
- 151 The β exponents for the intermediate and mobile amorphous components are stretching
- 152 parameters reflecting in the one hand dynamic heterogeneity, and on the other hand a partial
- 153 Gaussian character typical for dipolar dephasing originating from the dominance of residual dipolar
- 154 couplings in the short network chains (a discussion is given below). This explains why the β values
- 155 were always ranging between 1 and 2. The T_{2i} was around and below 0.1 ms in the network melt
- 156 down to 0.03 ms for fully crystallized samples, while T_{2m} was around 0.2, staying the same or even
- 157 increasing somewhat during crystallization. For the given short network chains, T_2 values are in the
- 158 range of 0.1 to 0.2 ms, which means that the mobile and intermediate components together reflect
- 159 reflect inhomogeneities of the network structure. As network chains become part of the crystal,
- 160 dangling defects with longer T_2 are left over, thus it increases in some cases.

4 **Results and Discussion**

4.1 High crystallinity and increase of $T_{\rm m}$ being related to crystal perfection

- 163 Our NMR-based crystallinity determination, applied to monitor isothermal crystallization of both
- 164 samples in Figure 1a,b confirms the initial WAXS-based observation that the samples reach high
- crystallinity of ~90% within a reasonably short time. This is an astonishingly high crystallinity for 165
- 166 polymer samples that are quiescently kept at room temperature, in particular considering the
- 167 disordered network structure and the short chains. The boric acid ester linkers are thus expected to be
- part of an ordered fold surface or to form intracrystalline layers, along the lines of recent studies of 168
- 169 linear precision polymers (Trigg et al., 2017; Marxsen et al., 2021). To reach such high crystallinity,
- 170 long-chain polymers are usually annealed at higher temperatures or shear aligned, and have to feature
- 171 fast chain mobility in the crystals (Schulz et al., 2022). For highly crosslinked networks, it is in fact a
- 172 peculiarity, as mentioned in the Introduction.

The crystallization kinetics $f_c(t)$ were evaluated by fits to the Avrami function (black solid lines in Figure 2a,b), which revealed Avrami exponents in the range between about 1 and 2. Since the variations were non-systematic across all our data (see also Figure 5 below), arising from uncertainties (noise) in the data at short times and possible secondary crystallization at longer times, we refrain from reporting and discussing the fitted exponents, but just report crystallization half times $t_{1/2}$. The values are 830 and 63 min for C_{10} and C_{12} , respectively, with the large difference mainly attributed to the different undercooling at 20°C. In both samples, the second moment continues to grow during crystallization, indicating a gradual densification or a suppression of fast small-angle motions. We thus interpret the observation in terms of an increase in crystal perfection, which, notably, takes place without further significant increase in crystallinity. The increase in enthalpy of melting previously reported (Soman et al., 2022a) can in this new light be attributed to the increasing crystal perfection observed from NMR rather than percent crystallinity.

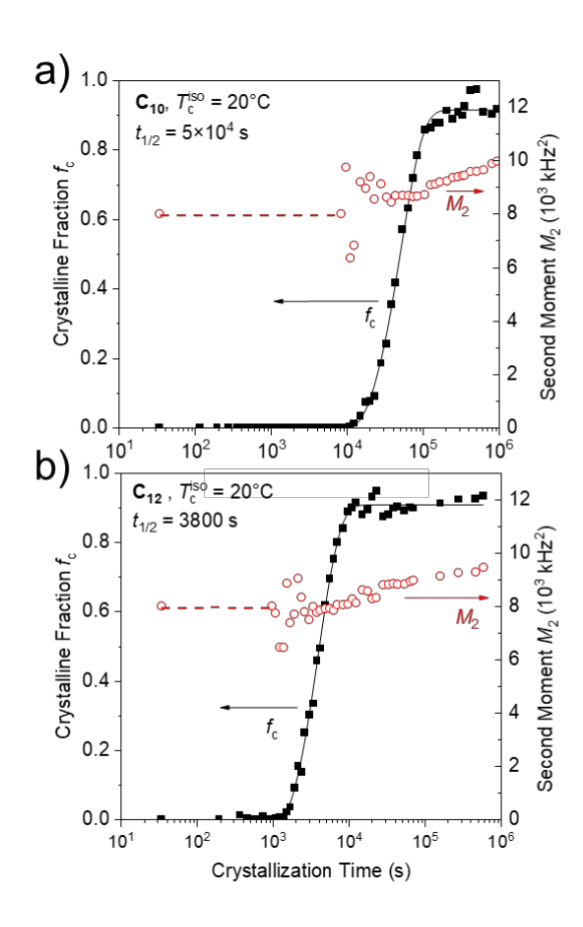


Figure 2. Crystalline fraction (f_c) and second moments of the crystalline lineshapes (M_2) plotted as a function of annealing time at 20 °C for the a) C_{10} and b) C_{12} ethylene vitrimers. The red dashed line indicates the time range where M_2 was fixed since stable fitting of a finite crystalline fraction was impossible. The black solid lines are fits to the Avrami function, from which we take the crystallization half time.

The crystallization of the networks was also tracked by WAXS over a 150 day crystallization period (**Figure 3a,b**). After 1 day of crystallization, the WAXS patterns already indicate a high crystallinity as inferred from the absence of an underlying amorphous halo which is observed in the scan of the amorphous network (0 min scan). In addition to the high crystallinity, the FWHM of the peaks does not show significant variation after the first day indicating a stable crystal size. At room temperature, the C_{10} eventually undergoes a spontaneous transformation from hexagonal to orthorhombic but not

within the first 30 days. In the C₁₂ network, the crystal structure appears to be hexagonal over the entire 150 day window and only transitions to orthorhombic at elevated temperatures of 65 °C (to be discussed later).

The M₂ values for hexagonal and orthorhombic crystals are distinct, and the NMR measurements reveal only hexagonal crystals in the first month consistent with the prior WAXS data. This is evidenced by the comparison of M₂ values for a C₁₀ sample crystallized isothermally at 20°C during heating and cooling with a rates of 1 K/m in **Figure 3c**. The first heating scan to 40°C reveals a slight decrease of M_2 in a range below $10^4 \, \text{kHz}^2$ (accompanied by only a slight decrease in crystallinity from about 0.92 to 0.86). The sample was then cooled again to room temperature, upon which the variation of M_2 is fully reversible, as evidenced by the second-heating data. Crystallinity actually diminishes above 48 °C, and annealing at 50 °C leads to a recrystallization into the orthorhombic phase (details to be discussed below in the context of Figure 6a). Importantly, this is directly reflected in the considerably larger M_2 value of around 1.2×10^4 kHz², which is now typical for similar crystal structures such as those of PE or aliphatic polyesters (Schäler et al., 2013). The orthorhombic crystallinity in the shown T range varies between 79 and 85%. The T-dependence of its M_2 is even weaker, and depends mostly on thermal expansion. The stronger dependence and lower values of the initial hexagonal phase may be related to enhanced dynamics such as increasing amplitude of local librations or conformational fluctuations (Schäler et al., 2013). It is noted that the M_2 values for the two phases are too close to allow for a separation of the fractions of either phase by fitting in samples where they coexist. However, in-between values can be interpreted qualitatively in terms of coexistence.

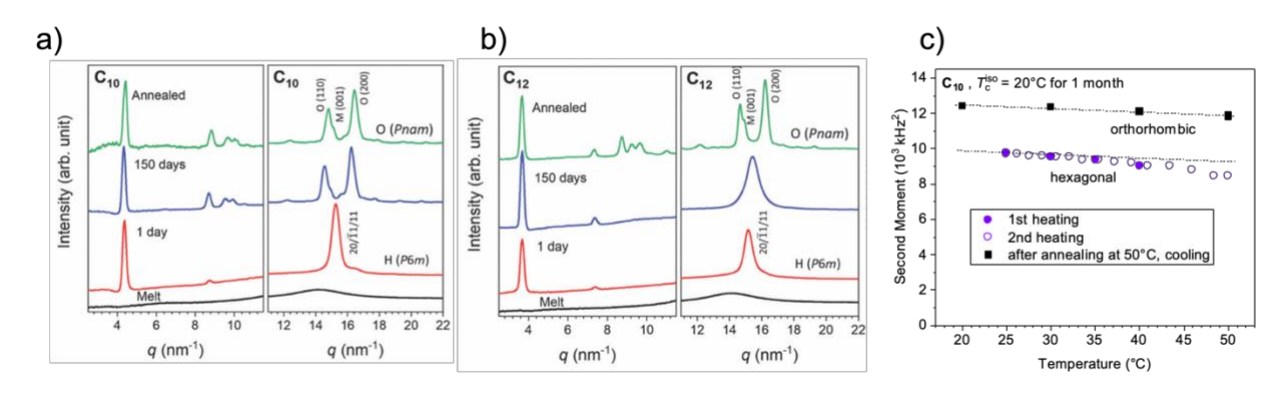
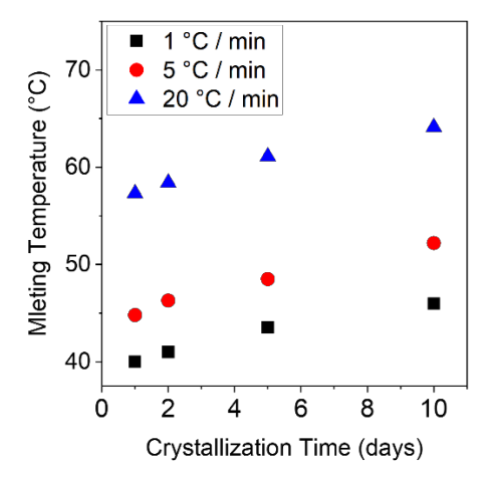


Figure 3. Time evolution of SAXS/WAXS spectra in the a) C_{10} and b) C_{12} networks at 23 °C revealing the transformations from hexagonal to orthorhombic unit cells which occur with time (in the C_{10} network) or heating to 65 °C (in the C_{12} network). Data reproduced from Soman et al., 2022a with permission. c) Second moment of the crystalline lineshape for the two relevant crystal structures as a function of temperature, recorded upon heating or cooling at 1 K/min. The parallel dashed lines indicate the typical weak decay due to thermal expansion of the lattice; the stronger and reversible decrease in the hexagonal phase indicates increased dynamics, e.g. increasing concentration of fluctuating conformational defects or librational motions.

Our previous report of increasing T_m with crystallization time corresponded to samples heated at a rate of 20 °C/min in the DSC (Soman et al., 2022a). In the present work, the time evolution of T_m was examined using different heating rates spanning from 0 to 20 °C/min. The DSC traces are shown in the Appendix (Figure A1). In all cases an increase is observed with essentially the same slope (Figure 4). Surprisingly, the value of T_m decreases significantly with slower heating rates, a phenomenon also observed in conventional linear PE (Hellmuth and Wunderlich, 1965). This puts the previous T_m results (Soman et al., 2022a), taken to be not too far from equilibrium, into

perspective. In that study, the increase in T_m was attributed to increasing crystallinity due to the change in the enthalpy of melting. Here, it is shown that increasing perfection leads to the increase in T_m . The higher apparent T_m values at 20 °C/min are thus attributed to the superheating of crystals, which refers to the ability to be heated above the equilibrium melting temperature (Hellmuth and Wunderlich, 1965). For polyethylene and polyoxymethylene used in that study, the superheating effect resulting in an ~4-5 °C shift for a range of heating rates from 0.6 to 20 °C/min. The effect is much larger in ethylene vitrimers. In the present work, we deduce from **Figure 4** that while the vitrimeric rearrangements and enhanced crystal perfection result in systems which are more stable and melt at higher $T_{\rm m}$, the superheating effect, apparent from the large differences between the different heating rates, is affected only little. We hypothesize that the melting kinetics are be governed by the timescale of vitrimeric rearrangements, which could be slower in the organized environment between the crystalline alkyl sheets. Note that the total time for a heating cycle ranges from 5 – 100 minutes depending on the ramp rate, and the rheological crossover time in the melt state is ~ 0.1 sec (Figure 1a), indicating ample time for relaxation events and bond exchange to modify





the samples during this ramp.

Figure 4. Melting temperatures of the C_{10} network as a function of crystallization time with different heating rates.

As noted in the Introduction, Kuenstler and Bowman (2023) found that thiol/thioester-based vitrimers with crystallizable C_{10} alkyl-dithiol linkers also show a long-time increase in T_m , the absolute value which is of the order of 20°C, thus much lower than in our case. T_m was higher for systems with faster bond-exchange kinetics. The annealing time dependence of T_m was not studied explicitly. The effect was attributed to potential lamellar thickening – which was not measured. This explanation must be reconciled with a system in which the disordered thioether/(thio)ester moieties are likely part of the lamellae and whose thickness is further bound by the crosslinks. In that work, the extended C_{10} units probably also crystallize in PE-type fashion similar to polymers with alkyl sidechains. Such a system, namely atactic poly(n-octadecyl methacrylate) was studied by Beiner and coworkers (Hempel et al., 2006), where a similar long-term increase of T_m was also observed. In that case, the C_{18} side-chains form interdigitated layered nanodomains separated by the disordered main chains, within which a hexagonal crystalline packing develops and was hypothesized to perfection over time, as detected by a slow increase of both T_m as well as the heat of melting. It remains an open question whether a thickening of an initially shorter crystallized stretch of the C_{18} (as depicted by Hempel et al.), or an improving organization/packing at the crystallite surface, is responsible for the

266

267268

269

270

271

272

273

274

275

276

277

278

279

280

281

282

283

284

Figure 5. a) C_{12} sample undergoes a crystal-crystal transition when annealed at 50 °C after isothermal crystallization at RT for 1 day. b) The C_{12} network directly cooled from the melt (150°C) transitions to the orthorhombic phase during isothermal crystallization at 50°C. The two black solid lines are Avrami fits excluding or assuming an onset time t_0 of 2.8×10^4 s. The two scenarios, providing Avrami exponents of 2.6 or 1.6, respectively, cannot be distinguished on the basis of the data/fitting quality.

4.2 Higher-temperature recrystallization and melting

As observed in the SAXS/WAXS data of **Figure 3**, the C_{12} sample can transition from hexagonal to orthorhombic when annealed at 65 °C. This transition was tracked using NMR on a C_{12} network first crystallized for 1 day followed by heating to 50 °C in 1700 s (rate of ~1 °C/min) as shown in **Figure 5a**, where we used the lower temperature so as to be able to compare with isothermal crystallization at the same temperature. This procedure leads to a minor partial melting, and then recrystallization into a denser phase (orthorhombic) but with almost the same crystallinity and a higher perfection. Notably, the M_2 values decrease first on heating from 20 to 50°C (see also **Figure 2c**), suggesting fast (but effectively small-angle) segmental fluctuations with increasing amplitude. Then, they steadily increase to the level expected for the orthorhombic crystal. The increase of M_2 can be

interpreted in terms of increasing crystalline perfection, or simply by a converted fraction. Taking the latter perspective, a conversion half time of 500 min is estimated.

This can be compared with the isothermal crystallization of the same network that is cooled directly from the melt to 50 °C, revealing a half time of about 1500 min (**Figure 5b**). This temperature is apparently below the equilibrium melting point of the hexagonal phase, but is above the annealing temperature required to form the orthorhombic phase. The hexagonal phase forms first (M_2 of around 8000 kHz²), and then gradually converts to the orthorhombic phase during the crystallization ($M_2 > 11$ kHz²). The crystallinity still reaches $f_c \sim 0.9$. The orthorhombic phase does not seem to directly nucleate and we note that this denser phase is effectively at a lower degree of undercooling than the hexagonal phase.

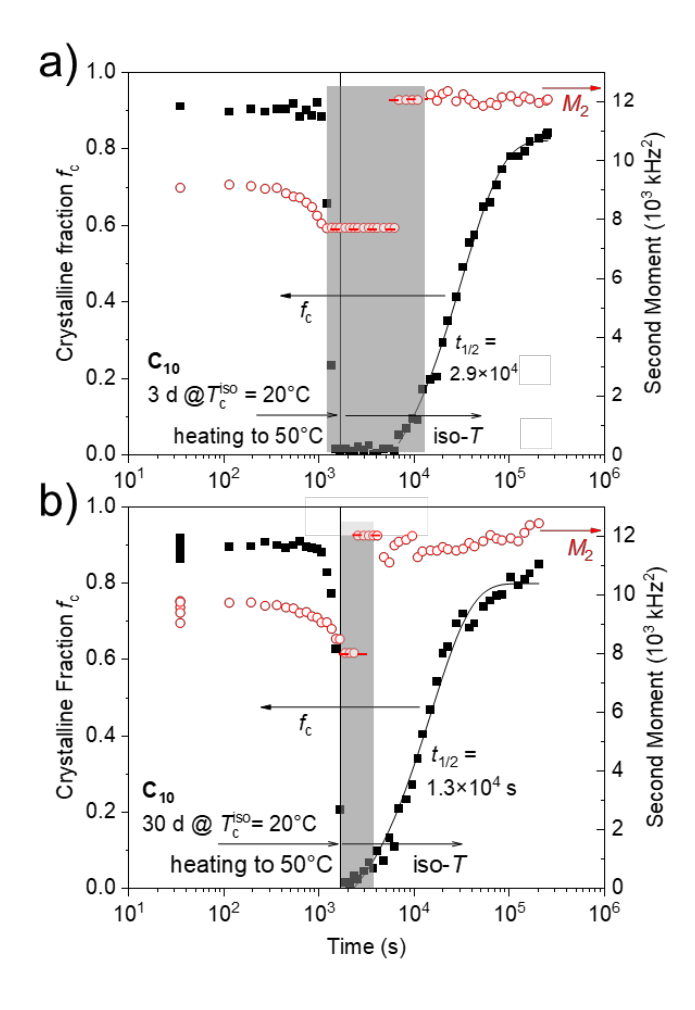


Figure 6. Memory effect on isothermal recrystallization at 50° C observed upon annealing of C_{10} a sample crystallized isothermally at 20° C for a) 3 days and b) 1 month. The latter has a stronger memory effect and thus faster crystallization (including a shorter apparent "induction time"). Note that isothermal crystallization at 50° C after cooling from the virgin melt is not observed on the given timescale.

4.3 Memory effect in vitrimer crystallization

Polymer crystals are known to have memory effects which can take long times to anneal out and fully erase thermal and processing history (Cheng et al., 1986; Bastiaansen et al., 1990; Hamad et al., 2015; Sangroniz et al., 2020). The C₁₀ network was first examined by crystallizing for 3 days or 1

month, followed by heating to 50° C (**Figure 6**). This temperature is above the melting point of the hexagonal phase initially formed on crystallization at lower temperatures (see **Figure 4**), and no crystallization directly into the orthorhombic phase was observed with several days at 50° C after cooling from the melt. As expected, both 20° C pre-crystallized samples show essentially complete melting upon heating to 50° C, yet this is now followed by recrystallization directly into the orthorhombic phase (as evidenced by the high and constant M_2). The 3-day sample (**Figure 6a**) shows a notable induction period, while the 1-month sample has an even stronger memory effect (**Figure 6b**) with an apparently shorter induction period and shorter overall crystallization half time. The orthorhombic phase apparently does not nucleate well (or not all all) and requires some "memory" facilitating its formation

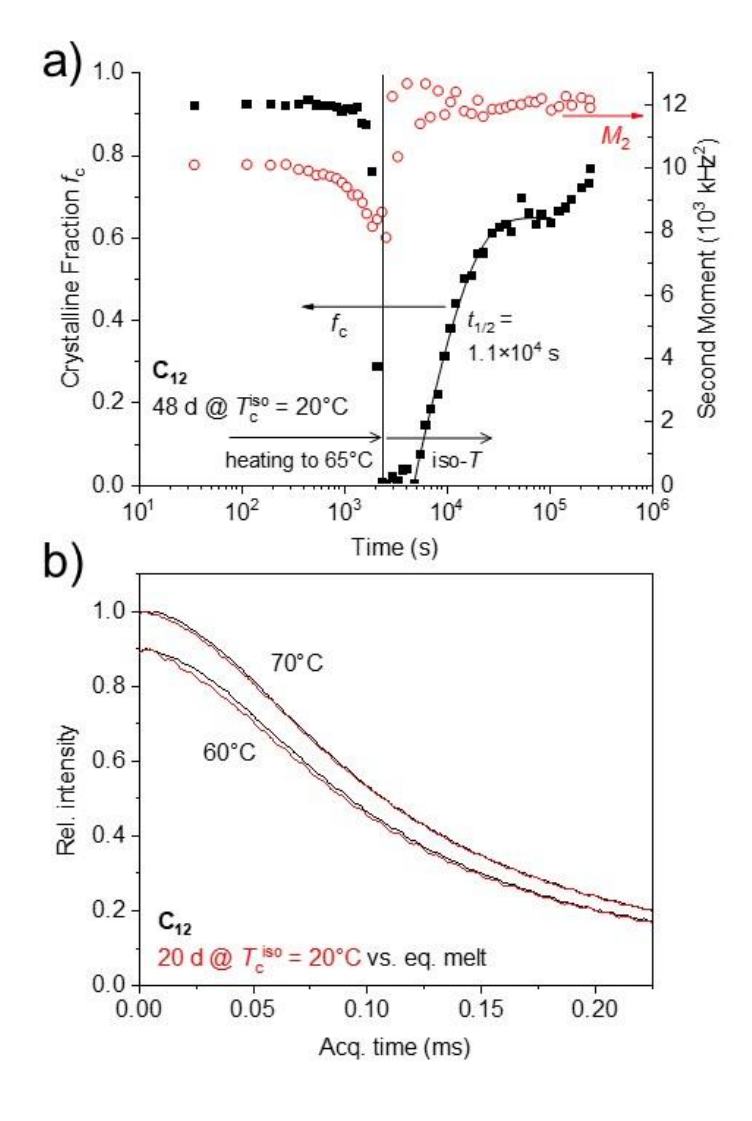


Figure 7. a) Memory effect of C_{12} on isothermal recrystallization at 65°C . b) MSE-FIDs at 60°C and 70°C; the latter was taken after 40 min. hold time at 60°C. The intensity data at 60°C is scaled by a factor of 0.9 for visual separation.

The C_{12} networks were also examined for memory effects, but heating to 50 °C is not sufficient to induce the same phenomena as in the C_{10} networks, as isothermal crystallization from the virgin melt and formation of (or transition into) the orthorhombic phase is already observed at this temperature (see **Figure 5 a,b**). We have thus focused on higher temperatures, where a sample crystallized at 20

- 322 °C for 1.5 months showing the hexagonal modification melts completely at 65 °C and recrystallizes
- 323 directly into the orthorhombic phase after a lag time of about 1.5 hours (Figure 7a). Qualitatively the
- 324 same behavior was observed for a sample crystallized at 20°C for 20 days after heating to 60°C,
- 325 where crystallization sets in already after about 20 min. (data not shown). In contrast, a virgin melt
- 326 cooled to the same temperatures did not crystallize.
- 327 As to the origin of this memory effect, one may consider an adapted network mesh topology
- 328 providing a "melt memory" with pre-arranged chains. This option is, however, unlikely, as the
- 329 memory is stable for hours, while the terminal (flow) time of the vitrimers, as governed by the bond-
- 330 exchange process, is well below the second scale (see Figure 1a). To test this hypothesis, or check
- 331 for the possible remainder of a small crystalline fraction, we compare in **Figure 7b** two (MSE-)FIDs
- 332 of melt states at 60°C and 70°C for a sample crystallized for 20 days with and without memory (the
- 333 latter taken after complete melting at 150°C for about 15 min.). For this experiment, the pre-
- 334 crystallized sample was held at 60°C for 40 min, during which time crystallization set in visibly. It
- 335 was then further heated to 70°C and held. The shown data are averages of the FIDs taken during the
- 336 induction times, where the signals did not change visibly and where no stable fitting of a finite
- 337 crystallinity was possible. Nevertheless, the direct comparison at 60°C with the data of the
- 338 equilibrated melt shows that the signal from the samples "with memory" is always decaying
- 339 somewhat more quickly, the data being compatible with a crystallinity degree on the percent level.
- 340 The effect is very small but still visible at 70°C, while at 80°C (with data taken after another 40 min
- 341 holding at 70°C) showed signals that are identical to those of the equilibrated melt within the noise.
- 342 Thus, the memory is most likely related to the existence of a very small fraction of high-melting
- 343 crystallites, possibly such ones for which the perfectioning has progressed more. We note that it is
- 344 expected that the observed differences pertain not just to a minute fraction of crystalline signal but a
- 345 somewhat decreased T_2 relaxation time of a part of the sample (i.e., the intermediate fraction in our
- 346 three-component fit), arising from some degree of immobilization of the chains surrounding the small
- 347 crystallites.
- 348 We finally add some comments on the shape of the melt-state FIDs, which could hold information on
- 349 a "melt memory". It is approximately Gaussian, as expected for very short network chains featuring
- 350 rather large residual dipolar coupling constants arising from the strongly anisotropic motions of the
- 351 short end-fixed chains (Saalwächter and Heuer, 2006). In other words, the transverse relaxation
- 352 process (normally characterized by a T_2 relaxation time) is rather pure dipolar dephasing, where an
- 353 orientational ("powder") average combined with multiple multi-spin couplings leads to the well-
- known Gaussian shape. In case of a homogeneous system, is described by $I(t) = \exp\{(9/40)D_{\text{res}}^2t^2\}$. 354
- 355 where D_{res} is the residual dipolar coupling, which is inversely proportional to the length of the
- 356 network strands (Saalwächter and Heuer, 2006). Since in our case D_{res} is large due to the short
- 357 strands (corresponding to a high crosslink density typical for thermosets), direct analysis of the FID,
- 358 which is normally precluded by field inhomogeneities and additional contributions of segmental
- 359 dynamics, becomes possible. Topological structures such as loops would contribute lower D_{res} and
- 360 the relaxation function would become modified/stretched, yet again, no differences are apparent
- 361 between the cases with and without memory.
- 362 Another relevant piece of information in this context is a nearly exponential long- T_2 tail, for which
- 363 fitting (not shown) provides a relative fraction of less than 10%. This corresponds to network defects,
- 364 whose rather low amplitude confirms the high conversion of the networks with its mostly 3-
- 365 functional crosslinks. More in-depth analysis into the network structure and a more stable fitting is
- 366 possible by using multiple-quantum (MQ) NMR, along the lines of our previous work (Saalwächter

and Heuer, 2006). Results along these lines are deferred to a future publication, where we focus on stoichiometrically imbalanced, defect-containing samples.

370 **5** Conclusions

- The crystallization of ethylene vitrimers was investigated by time-domain NMR to probe the kinetics,
- perfection, and polymorphic transitions of these systems. NMR analysis confirms that the
- 373 crystallinity is very high, of order 90%, in agreement with prior WAXS data. A notable and
- significant long-time increase of $T_{\rm m}$ upon annealing was shown to not be related to an increase in
- 375 crystallinity (reaching its final level comparably quickly) but rather to an increased crystal perfection,
- enabled by a reorganization of the dynamic bonds on the surface of the crystalline alkyl layers. The
- dynamic bonds thus become part of a layered crystal structure, as also evidenced by a sharp SAXS
- peak reflecting the boric ester layer spacing.
- These results may be of general relevance for systems in which alkyl nanodomains can crystallize.
- Both in a recent study of somewhat more complex C₁₀-based vitrimers (Kuenstler and Bowman,
- 381 2023) and in a linear methacrylate polymer with C_{18} side-chains (Hempel et al., 2006), similar $T_{\rm m}$
- increases were reported. In the latter case, the melting enthalpy change over time was also studied by
- DSC, and shown to increase along with $T_{\rm m}$, in the same way as in our ethylene vitrimers (Soman et
- al., 2022a). We could here show that this increase is not related to increased cystallinity but is rather
- related to perfectioning of the layers containing the crosslinks, meaning that the surface energy is
- reduced. This emphasizes the relevance of our NMR investigations, providing a robust measure of
- 387 the degree of crystallinity.
- NMR also allows us to follow the polymorphic transition from hexagonal to orthorhombic based on
- the dipolar second moment of the crystalline lineshape, originating from slightly different proton
- densities and being detected in terms of differences in transverse relaxation times. We further
- identified a strong superheating effect, where higher heating rates lead to significantly higher
- apparent $T_{\rm m}$ values as the samples are heated beyond their equilibrium melting temperature. The
- related sluggish melting kinetics may be tied to a slower dynamic bond exchange in the crystalline
- interlayers. This finding suggests that it is generally difficult in the given system, as well as in related
- ones (Kuenster and Bowman, 2023; Hempel et al., 2006), to measure and draw conclusions from –
- 396 the actual melting temperature of the given structure.
- 397 The vitrimers are finally shown to exhibit strong memory effects, where our NMR observations are
- compatible with a small remaining high-melting fraction of well-optimized crystals that can nucleate
- 399 the crystallization directly into the orthorhombic phase. In summary, our study has provided key new
- 400 insights into the role of dynamic bonds on crystallization in dense networks, that would typically not
- 401 crystallize despite being made up of monodisperse building blocks. Future work is directed towards
- 402 introducing controlled defects and studying their impact on terminal flow and on semicrystalline
- 403 structure formation.

404

6 Conflict of Interest

405

408

412

420

424

425

426

427

The authors declare that the research was conducted in the absence of any commercial or financial relationships that could be construed as a potential conflict of interest.

7 Author Contributions

- Synthesis of vitrimers, X-ray scattering, rheology, and calorimetery were performed by B.S. All
- NMR experiments, fitting, and analyses were performed by K.S. The project idea, development, and
- writing of the manuscript was contributed by all authors.

8 Funding

- This work was partially supported by the National Science Foundation through award CBET-
- 414 2029928 (B.S. and C.M.E.). Partial funding was also provided by the Deutsche
- 415 Forschungsgemeinschaft (DFG) in the framework of the SFB-TRR 102 (project-ID 189853844),
- 416 project A1 (K.S.).

417 9 Acknowledgments

- We acknowledge the use of the facilities at the Materials Research Laboratory at the University of
- 419 Illinois, Urbana-Champaign.

10 Data Availability Statement

- The datasets [GENERATED/ANALYZED] for this study can be found in the [NAME OF
- 422 REPOSITORY] [LINK]. [will be added upon final submission]

423 11 Appendix

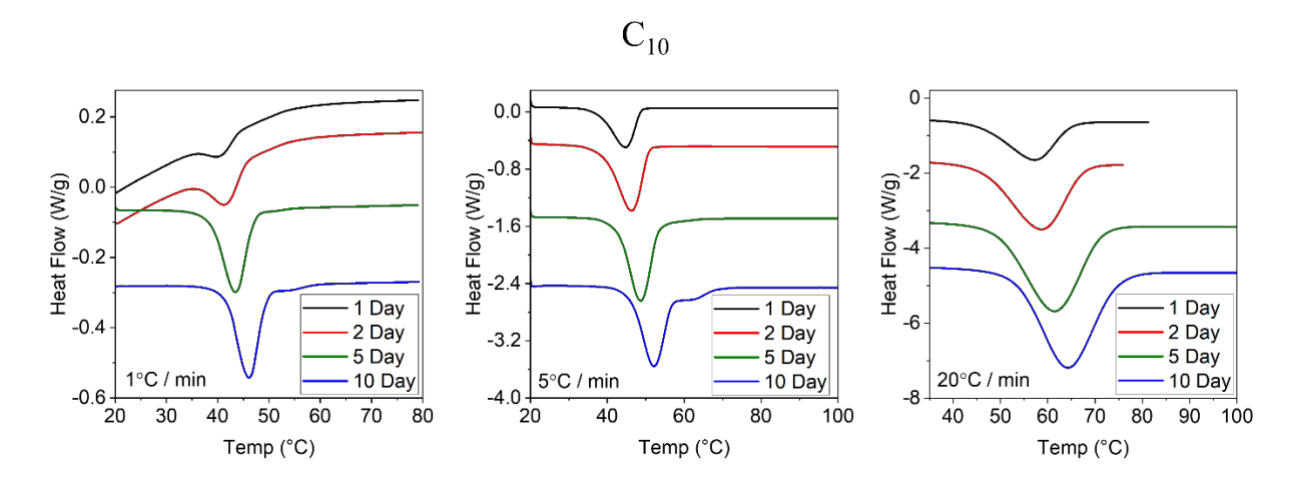


Figure A1. DSC heating traces of C₁₀ crystallized isothermally at 20°C for different durations (1-10 days), using different heating rates of 1 (left), 5 (middle) and 20 °C/min (right).

428 12 References

- Bastiaansen, C., Meyer, H., and Lemstra, P. (1990). Memory effects in polyethylenes: influence of processing and crystallization history. *Polymer* 31, 1435-1440.
- Chen, F., Cheng, Q., Gao, F., Zhong, J., Shen, L., Lin, C., and Lin, Y. (2021). The effect of latent plasticity on the shape recovery of a shape memory vitrimer. *European Polymer Journal* 147, 110304.
- Chen, Q., and Kurosu, H. (2007). Solid-state NMR studies on semicrystalline polymers. *Annual Reports on NMR Spectroscopy* 61, 247-281.
- Cheng, S.Z., Cao, M., and Wunderlich, B. (1986). Glass transition and melting behavior of poly (oxy-1, 4-phenyleneoxy-1, 4-phenylenecarbonyl-1, 4-phenylene)(PEEK). *Macromolecules* 19, 1868-1876.
- Denissen, W., Droesbeke, M., Nicolaÿ, R., Leibler, L., Winne, J.M., and Du Prez, F.E. (2017).

 Chemical control of the viscoelastic properties of vinylogous urethane vitrimers. *Nature communications* 8, 14857.
- Denissen, W., Rivero, G., Nicolaÿ, R., Leibler, L., Winne, J.M., and Du Prez, F.E. (2015). Vinylogous urethane vitrimers. *Advanced Functional Materials* 25, 2451-2457.
- El-Zaatari, B.M., Ishibashi, J.S., and Kalow, J.A. (2020). Cross-linker control of vitrimer flow. *Polymer Chemistry* 11, 5339-5345.
- Ezquerra, T.A., Majszczyk, J., Baltà-Calleja, F.J., López-Cabarcos, E., Gardner, K., and Hsiao, B.
 (1994). Molecular dynamics of the α relaxation during crystallization of a glassy polymer: A
 real-time dielectric spectroscopy study. *Physical Review B* 50, 6023.
- Golitsyn, Y., Pulst, M., Samiullah, M.H., Busse, K., Kressler, J., and Reichert, D. (2019).
 Crystallization in PEG networks: The importance of network topology and chain tilt in crystals. *Polymer* 165, 72-82.
- Gu, W., Li, F., Liu, T., Gong, S., Gao, Q., Li, J., and Fang, Z. (2022). Recyclable, Self-Healing Solid Polymer Electrolytes by Soy Protein-Based Dynamic Network. *Advanced Science* 9, 2103623.
- Guerre, M., Taplan, C., Winne, J.M., and Du Prez, F.E. (2020). Vitrimers: directing chemical reactivity to control material properties. *Chemical science* 11, 4855-4870.
- Hamad, F.G., Colby, R.H., and Milner, S.T. (2015). Lifetime of flow-induced precursors in isotactic polypropylene. *Macromolecules* 48, 7286-7299.
- Hellmuth, E., and Wunderlich, B. (1965). Superheating of linear high-polymer polyethylene crystals.
 Journal of Applied Physics 36, 3039-3044.
- Hempel, E., Budde, H., Höring, S., Beiner, M. (2006). On the crystallization behavior of frustrated
 alkyl groups in poly(*n*-octadecyl methacrylate). *Journal of Non-Crystalline Solids* 352, 5013 5020
- Hubbard, A.M., Ren, Y., Konkolewicz, D., Sarvestani, A., Picu, C.R., Kedziora, G.S., Roy, A.,
 Varshney, V., and Nepal, D. (2021). Vitrimer transition temperature identification: coupling various thermomechanical methodologies. *ACS Applied Polymer Materials* 3, 1756-1766.

- Hubbard, A.M., Ren, Y., Picu, C.R., Sarvestani, A., Konkolewicz, D., Roy, A.K., Varshney, V., and
 Nepal, D. (2022). Creep mechanics of epoxy vitrimer materials. *ACS Applied Polymer Materials* 4, 4254-4263.
- Ishibashi, J.S., Pierce, I.C., Chang, A.B., Zografos, A., El-Zaatari, B.M., Fang, Y., Weigand, S.J.,
 Bates, F.S., and Kalow, J.A. (2021). Mechanical and structural consequences of associative
 dynamic cross-linking in acrylic diblock copolymers. *Macromolecules* 54, 3972-3986.
- Jing, B.B., and Evans, C.M. (2019). Catalyst-free dynamic networks for recyclable, self-healing solid polymer electrolytes. *Journal of the American Chemical Society* 141, 18932-18937.
- Kloxin, C.J., and Bowman, C.N. (2013). Covalent adaptable networks: smart, reconfigurable and responsive network systems. *Chemical Society Reviews* 42, 7161-7173.
- Krishnan, B.P., Saalwaechter, K., Adjedje, V.K., and Binder, W.H. (2022). Design, Synthesis and
 Characterization of Vitrimers with Low Topology Freezing Transition Temperature.
 Polymers 14, 2456.
- Kuenstler, A.S. and Bowman, C.N. (2023) Catalytic control of crystallization in dynamic networks.
 ACS Macro Letters 12, 133-139
- 482 Lin, Y., Chen, Y., Yu, Z., Huang, Z., Lai, J.-C., Tok, J.B.-H., Cui, Y., and Bao, Z. (2022).
 483 Reprocessable and recyclable polymer network electrolytes via incorporation of dynamic covalent bonds. *Chemistry of Materials* 34, 2393-2399.
- Luo, J., Demchuk, Z., Zhao, X., Saito, T., Tian, M., Sokolov, A.P., and Cao, P.-F. (2022). Elastic vitrimers: Beyond thermoplastic and thermoset elastomers. *Matter* 5, 1391-1422.
- Lv, G., Li, X., Jensen, E., Soman, B., Tsao, Y.-H., Evans, C.M., and Cahill, D.G. (2023). Dynamic Covalent Bonds in Vitrimers Enable 1.0 W/(m K) Intrinsic Thermal Conductivity.

 Macromolecules 56, 1554-1561.
- Ma, J., Porath, L.E., Haque, M.F., Sett, S., Rabbi, K.F., Nam, S., Miljkovic, N., and Evans, C.M.
 (2021). Ultra-thin self-healing vitrimer coatings for durable hydrophobicity. *Nature Communications* 12, 5210.
- Marxsen, S.F., Häußler, M., Mecking, S., Alamo, R.G. (2021) Unlayered–layered crystal transition in recyclable long-spaced aliphatic Polyesters. *ACS Applied Polymer Materials* 3, 5243-5256.
- Maus, A., Hertlein, C., Saalwächter, K. (2006) A robust proton NMR method to investigate hard/soft
 ratios, crystallinity, and component mobility in polymers. *Macromolecular Chemistry and Physics* 207, 1150-1158
- Montarnal, D., Capelot, M., Tournilhac, F., and Leibler, L. (2011). Silica-like malleable materials from permanent organic networks. *Science* 334, 965-968.
- Niu, W., Zhang, Z., Chen, Q., Cao, P.-F., and Advincula, R.C. (2021). Highly recyclable,
 mechanically isotropic and healable 3D-printed elastomers via polyurea vitrimers. ACS
 Materials Letters 3, 1095-1103.
- Pascual-Jose, B., De La Flor, S., Serra, A., and Ribes-Greus, A. (2023). Analysis of Poly (thiourethane) Covalent Adaptable Network through Broadband Dielectric Spectroscopy. *ACS Applied Polymer Materials*.
- Porath, L., Huang, J., Ramlawi, N., Derkaloustian, M., Ewoldt, R.H., and Evans, C.M. (2022).
 Relaxation of Vitrimers with Kinetically Distinct Mixed Dynamic Bonds. *Macromolecules* 4450-4458.

- Porath, L.E., and Evans, C.M. (2021). Importance of broad temperature windows and multiple rheological approaches for probing viscoelasticity and entropic elasticity in vitrimers.
- 511 *Macromolecules* 54, 4782-4791.
- Ricarte, R.G., and Shanbhag, S. (2021). Unentangled vitrimer melts: interplay between chain relaxation and cross-link exchange controls linear rheology. *Macromolecules* 54, 3304-3320.
- Rossegger, E., Höller, R., Reisinger, D., Fleisch, M., Strasser, J., Wieser, V., Griesser, T., and Schlögl, S. (2021). High resolution additive manufacturing with acrylate based vitrimers using organic phosphates as transesterification catalyst. *Polymer* 221, 123631.
- Röttger, M., Domenech, T., Van Der Weegen, R., Breuillac, A., Nicolaÿ, R., and Leibler, L. (2017).
 High-performance vitrimers from commodity thermoplastics through dioxaborolane
 metathesis. *Science* 356, 62-65.
- Saalwächter, K., and Heuer, A. (2006). Chain dynamics in elastomers as investigated by proton multiple-quantum NMR. *Macromolecules* 39, 3291-3303.
- 522 Sangroniz, L., Cavallo, D., and Müller, A.J. (2020). Self-nucleation effects on polymer crystallization. *Macromolecules* 53, 4581-4604.
- Schäler, K., Achilles, A., Bärenwald, R., Hackel, C., and Saalwächter, K. (2013). Dynamics in crystallites of poly (ε-caprolactone) as investigated by solid-state NMR. *Macromolecules* 46, 7818-7825.
- Schäler, K., Roos, M., Micke, P., Golitsyn, Y., Seidlitz, A., Thurn-Albrecht, T., Schneider, H.,
 Hempel, G., Saalwächter, K. (2015) Basic principles of static proton low-resolution spin
 diffusion NMR in nanophase-separated materials with mobility contrast. *Solid State Nuclear Magnetic Resonance* 72, 50-63
- Schulz, M., Schäfer, M., Saalwächter, K., Thurn-Albrecht, T. (2022) Competition between crystal
 growth and intracrystalline chain diffusion determines the lamellar thickness in
 semicrystalline polymers. *Nature Communications* 13, 119.
- Soccio, M., Nogales, A., Lotti, N., Munari, A., and Ezquerra, T.A. (2007). Evidence of early stage precursors of polymer crystals by dielectric spectroscopy. *Physical Review Letters* 98, 037801.
- Soman, B., and Evans, C.M. (2021). Effect of precise linker length, bond density, and broad temperature window on the rheological properties of ethylene vitrimers. *Soft Matter* 17, 3569-3577.
- Soman, B., Go, Y.K., Shen, C., Leal, C., and Evans, C.M. (2022a). Impact of dynamic covalent chemistry and precise linker length on crystallization kinetics and morphology in ethylene vitrimers. *Soft Matter* 18, 293-303.
- Soman, B., Schweizer, K.S., and Evans, C.M. (2022b). Fragile Glass Formation and Non-Arrhenius Upturns in Ethylene Vitrimers Revealed by Dielectric Spectroscopy. *Macromolecules*.
- Sonnenberger, N., Anders, N., Golitsyn, Y., Steinhart, M., Enke, D., Saalwächter, K., and Beiner, M. (2016). Pharmaceutical nanocrystals confined in porous host systems—interfacial effects and amorphous interphases. *Chemical Communications* 52, 4466-4469.
- Tanaka, H., and Nishi, T. (1986). Study of crystallization process of polymer from melt by a realtime pulsed NMR measurement. *The Journal of chemical physics* 85, 6197-6209.

- Trigg, E.B., Stevens, M.J., and Winey, K.I. (2017). Chain folding produces a multilayered morphology in a precise polymer: simulations and experiments. *Journal of the American Chemical Society* 139, 3747-3755.
- Van Lijsebetten, F., Engelen, S., Bauters, E., Van Vooren, W., Smulders, M.M., and Du Prez, F.E. (2022). Recyclable vitrimer epoxy coatings for durable protection. *European Polymer Journal* 176, 111426.
- Van Zee, N.J., and Nicolaÿ, R. (2020). Vitrimers: Permanently crosslinked polymers with dynamic network topology. *Progress in Polymer Science* 104, 101233.
- Wibowo, E.S., and Park, B.-D. (2020). Determination of crystallinity of thermosetting ureaformaldehyde resins using deconvolution method. *Macromolecular Research* 28, 615-624.
- Wurm, A., Soliman, R., Goossens, J., Bras, W., and Schick, C. (2005). Evidence of pre-crystalline order in super-cooled polymer melts revealed from simultaneous dielectric spectroscopy and
 SAXS. *Journal of non-crystalline solids* 351, 2773-2779.
- Yan, P., Zhao, W., Zhang, B., Jiang, L., Petcher, S., Smith, J.A., Parker, D.J., Cooper, A.I., Lei, J.,
 and Hasell, T. (2020). Inverse vulcanized polymers with shape memory, enhanced mechanical
 properties, and vitrimer behavior. *Angewandte Chemie International Edition* 59, 13371 13378.
- Zheng, J., Png, Z.M., Ng, S.H., Tham, G.X., Ye, E., Goh, S.S., Loh, X.J., and Li, Z. (2021).
 Vitrimers: Current research trends and their emerging applications. *Materials Today* 51, 586-625.

570